Ant-colony optimization-based multi-input multi-output (ACO-MIMO) equalization for low-complexity mode-division multiplexing (MDM) processing

TIANFENG ZHAO,[1] FENG WEN,[1,*] BIANXIA FENG,[1] FENG TIAN,[2] MINGMING TAN,[3] BAOJIAN WU,[1] BO XU,[1] AND KUN QIU[1]

[1]*Key Lab of Optical Fiber Sensing and Communication, Ministry of Education, University of Electronic Science and Technology of China, Chengdu 611731, China*
[2]*State Key Laboratory of Information Photonics and Optical Communications, Beijing University of Posts and Telecommunications, Beijing 100876, China*
[3]*Aston Institute of Photonics Technologies, Aston University, Birmingham B4 7ET, UK*
[*]*fengwen@uestc.edu.cn*

Abstract: In mode-division multiplexing (MDM) systems, the computational complexity of the multi-input multi-output (MIMO) equalization module is a critical obstacle to practical development. The step size μ and the number of taps K are key parameters in the equalization algorithm, influencing the performance of finite impulse response (FIR) equalizers, including convergence speed and output signal quality. To alleviate the computational burden of locating the optimal μ-K combination, we propose two ant colony optimization (ACO) -based MIMO equalization schemes: the fixed ACO-MIMO and the random ACO-MIMO, corresponding to two optimization strategies. These schemes expedite the initialization process of both parameters. Subsequently, we conduct experiments to evaluate their performance in a 3-mode recirculating-loop transmission system. Our findings demonstrate that, compared to conventional schemes, such as genetic algorithm (GA) and steepest descent algorithm (SDA), the proposed ACO-MIMO schemes significantly reduce the number of calls to the equalization algorithm for locating optimal μ-K combination by up to 42.74% and 80.63%, reducing the complexity of the whole MIMO equalization for MDM systems. And the resulting hit-rate P_{hit} for the optimal μ-K combination reaches up to 99.34%. Moreover, the ACO-MIMO schemes exhibit stable performance across different data collected from various round-trips, confirming the robust operation for the long-haul MDM transmission. Finally, we investigate the performance disparity between the two proposed ACO-MIMO schemes through bit-error-rate (BER) distribution, concluding that under a large dataset with various BER distributions, the performance of both schemes is essentially equivalent.

1. Introduction

Mode-division multiplexing (MDM) technology, utilizing few-mode fiber (FMF), holds significant promise for achieving high-capacity parallel transmission across spatial mode channels. It emerges as a leading contender for next-generation fiber-optic communication systems, offering potential breakthroughs beyond the nonlinear Shannon limit [1–3]. However, the signal quality in MDM systems is significantly affected by distortions arising from various mode channels, including mode coupling and differential mode group delay (DMGD). To address these spatial-mode related distortions, the integration of a multi-input multi-output (MIMO) module featuring butterfly-shaped finite impulse response (FIR) equalizers is essential for digital signal processing (DSP) at the receiver [4–6]. In the adaptive equalization algorithm within the MIMO module, the selected values of crucial parameters, e.g., the step size μ and taps number K, dictate the performance of the equalizers. In MDM systems experiencing pronounced fluctuations over time [7–9], it's

essential to adaptively adjust these parameters as the channel conditions evolve, enabling better utilization of the compensation function. Locating the best combination of μ-K is crucial for ensuring consistent communication quality within the system and for optimizing network load distribution based on communication performance. Hence, computational complexity in MIMO modules involves two key aspects:

1. The complexity needed to initialize the μ-K parameter space;

2. The complexity associated with executing the equalization function, such as training the equalizers and generating output signals.

As the number of transmitted modes increases, the complexity induced by MIMO equalization grows exponentially, severely impeding the transmission performance of MDM systems. And minimizing MIMO complexity is crucial for advancing the commercialization of MDM technology.

Recent research on reducing MIMO complexity has predominantly focused on the second aspect. An unconstrained adaptive frequency-domain least mean square (FD-LMS) algorithm was proposed for MDM transmission [10], aimed at compressing the redundant FFT/IFFT during the training process. Additionally, a training-aided frequency domain equalizer (FDE) was proposed based on channel estimation through constant-amplitude zero-auto-correlation (CAZAC) codes. The proposed scheme exhibited a convergence speed 4.48 times faster than typical FD-LMS-based equalization in a 3-mode multiplexing system [11]. While these schemes notably reduced MIMO complexity for equalizer convergence, the complexity arising from multiple calls to the equalization algorithm during parameter initialization (e.g., μ and K) remains significant. To alleviate the dependence of equalization performance on the initial μ-K values, step-variable and taps-variable equalization algorithms were proposed. These methods demonstrated higher training efficiency and reduced residual error [12–14]. However, the complexity issue arising from the initialization of additional hyper-parameters remains inevitable.

In this paper, to address the first aspect of MIMO complexity, we integrate the ant-colony optimization (ACO) algorithm into MIMO operations. We propose two ACO-MIMO equalization schemes, namely fixed and random ACO-MIMOs, aimed at reducing the number of calls to the FD-LMS algorithm used to locate the optimal μ-K combination. To validate the performance of these schemes, we establish a 3-mode multiplexed recirculating-loop experimental system based on a 10 km-length FMF, as in our previous works [15]. Implementing the proposed algorithms at the receiver side, both fixed and random ACO-MIMO schemes achieve high hit-rates (P_{hit}) for optimal parameters, reaching up to 99.34% and 97.7%, respectively. Compared to genetic algorithm (GA) and steepest descent algorithm (SDA), the average number of calls to the FD-LMS algorithm (referred to as C_{LMS}) required to reach the optimal μ-K combination is significantly reduced by the ACO-MIMO schemes, by up to 42.74% and 80.63%, respectively. Furthermore, the proposed schemes exhibit robust performance across varying transmission distances. When considering data with different round-trips, the ACO-MIMO schemes achieve maximum C_{LMS} reductions of 28.97% and 26.16% after full evolution compared to GA. Finally, we explore the relationship between the performance of the two ACO-MIMO schemes and the distribution of bit-error rate (BER).

The rest part of this paper is arranged as follows: in Section 2, we provide the detailed operation of both the fixed and the random ACO-MIMO schemes; Section 3 outlines the experimental setup of the FMF recirculating loop system and describes the corresponding device properties; then, in Section 4, based on the experimental results, we investigate the performance of the two ACO-MIMO schemes from various perspectives, including the hit rate of optimal parameters, distribution characteristics of the BER output, and the required number of calls to the equalization algorithm; finally, the conclusions are drawn in Section 5.

2. Principle of ACO-MIMO scheme

The feedback training algorithm stands as the cornerstone of the MIMO equalization module, categorized into data-aided and non-data-aided types [16,17]. Compared to the non-data-aided algorithms, data-aided algorithms prove more adept for MDM systems due to their faster and steadier convergence. In this paper, we employ the FD-LMS algorithm, falling under the data-aided category, as our equalization algorithm. In the FD-LMS algorithm, μ represents the step size factor, while K denotes the number of taps [10]. During training, μ directly influences feedback behavior as a multiplication coefficient, whereas K determines the size of each processed data block. Therefore, the μ-K combination's value heavily influences MIMO equalization performance. Excessive calls to the FD-LMS algorithm for μ-K localization can incur substantial computational overhead, thereby diminishing MIMO equalization efficiency. Consequently, finding an efficient method to determine the optimal μ-K combination remains an ongoing issue for MIMO equalization processing in high-capacity MDM systems, especially considering nearly 1000 modes [18].

The ACO algorithm is primarily employed to address the traveling salesman problem (TSP) through imitating the ant's sensitivity to the pheromone, which is left by the crawling ants and gradually evaporated [19,20]. And the ants prefer the path with higher pheromone concentrations. Over time, through the iterative process of ant evolution, the optimal path accumulates the most pheromones due to positive feedback mechanisms. Consequently, the ACO algorithm is insensitive to the initial state of ants, rendering it more robust. Additionally, due to these characteristics, the ACO algorithm is well-suited for solving extreme points of multivariate functions [21,22]. In this scenario, pheromone is correlated with the function value and determines the ant's subsequent search behavior, that is whether the local search or global search. Thus, the ants in ACO algorithm operate in parallel and exhibit self-organizing. In MIMO equalization, distinct μ-K combinations correspond to varying BER outputs, offering the potential to substantially diminish computational overhead in locating the optimal μ-K combination by integrating the ACO algorithm into MIMO equalization.

We enhance the ACO algorithm and introduce two ACO-MIMO schemes, each employing fixed and random movement directions to execute distinct local search strategies. These schemes are respectively referred to as the fixed and random ACO-MIMOs. The ACO-MIMO schematic diagram is depicted in Fig. 1. We divide the ACO-MIMO process into two parts: the basic outline and the updating policy. The pseudocode of the basic outline, labeled as Algorithm 1, is presented below. We define the number of ants in ACO-MIMO as N and the evolution times as G. Initially, all ants are randomly positioned on the BER distribution plane, where each point (x,y) in Cartesian Coordinates represents a μ-K combination. Each ant independently calls the FD-LMS function to compute the BER corresponding to its μ-K combination. The pheromone of the nth ant's initial coordinate is defined as $\tau_n(0) = 0.5 - BER^n(0)$, where $BER^n(0)$ represents the BER at the initial coordinate of the nth ant. It indicates that higher pheromone concentration corresponds to lower BER values, making the corresponding coordinate points more attractive to the ants. Throughout the entire evolutionary process, we assume ants are initialized only once, and subsequent state changes are related to previous states. After the tth evolution, the pheromone of the nth ant's coordinate $\tau_n(t)$ is updated according to Eq. (1), where ρ represents the evaporation factor of the pheromone and is assigned as 0.9 [21,22]. In addition, $BER^n(t)$ represents the BER of the coordinate point for the nth ant after t times evolutions.

$$\tau_n(t) = (1 - \rho) \times \tau_n(t - 1) + [0.5 - BER^n(t)]. \qquad (1)$$

Then, during the tth evolution, the nth ant determines whether to perform global or local search for the next step based on the individual transfer probability $P^n_{tran}(t)$ calculated by Eq. (2) [23], where $\tau_{max}(t)$ represents the maximum pheromone concentration among the coordinate points of the population after the tth evolution. We set P_0 as the transfer probability threshold.

Typically, higher pheromone concentration corresponds to lower BER. Since BER does not exhibit significant fluctuations with respect to μ-K, when the of pheromone concentration is high enough such that $P^n_{tran} < P_0$, it indicates a higher probability of finding the optimal μ-K combination near the ant's vicinity, thus prompting local search. Conversely, when the pheromone concentration at the coordinate of the ant is low (i.e., $P^n_{tran}(t) > P_0$), it suggests a higher BER in the ant's coordinate, making it unsuitable for local search and hence turning to global search. Additionally, according to Eq. (2), the maximum pheromone concentration $\tau_{max}(t)$ in the population also affects the ants' search behavior. A higher $\tau_{max}(t)$ requires ants to have a higher $\tau_n(t)$ for their transfer probability to exceed P_0, thereby enabling local search. Therefore, at this point, the pheromone concentration determines search range for the ants. The updating policies of the fixed and random ACO-MIMO schemes are also shown below, which are titled as Algorithm 2 and Algorithm 3, respectively. To explore more possibilities and avoid falling into the local optima, the ants randomly select the candidate coordinate during global search. Notably, the difference between the updating policies of the two ACO-MIMO schemes lies in the local search method. When the BER of the selected candidate point is lower than the current BER, the ant moves to the candidate point; otherwise, the candidate point is added to the blacklist. Afterward, the algorithm concludes and outputs the minimum BER in the population when the evolving population meets the termination condition; otherwise, it initiates the next evolution.

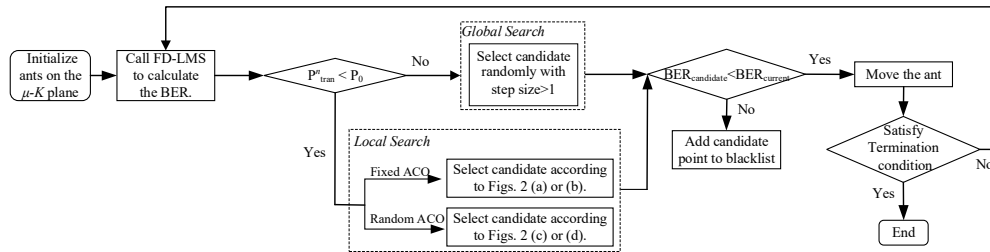$$P^n_{tran}(t) = \frac{\tau_{max}(t) - \tau_n(t)}{\tau_{max}(t)}. \tag{2}$$

Fig. 1. ACO-MIMO schematic diagram.

Algorithm 1. Basic ACO-MIMO outline.

1	set ACO parameters
2	perform MIMO equalization for the μ-K coordinate of each ant
3	initialize pheromone levels based on the MIMO results
4	**for** $g = 1$ to G **do**
5	**for** $n = 1$ to N **do**
6	determine location of the next step based on the updating policy
7	**end for**
8	record the minimum BER output
9	update pheromone levels according to Eq. (1)
10	**end for**
11	output the minimum BER

In the local search of ACO-MIMO scheme, we define the movement direction from the previous coordinate point to the current point as the arrival direction for the ant. Therefore, in addition to the arrival direction, local search includes 7 coordinate points as candidates for the next hop, corresponding to 7 movement directions. In the fixed ACO-MIMO scheme, the

Algorithm 2. Fixed ACO-MIMO updating policy.

1	**for** $n = 1$ to N **do**
2	produce the P_{tran}^n
3	**if** $P_{tran}^n < P_0$ **then**
4	determine the candidate point based on the direction priority depicted in Figs. 2 (a) or (b)
5	perform MIMO equalization for the candidate point
6	**if** BER of the candidate point < BER of the current point **then**
7	the ant moves to the candidate point
8	**else**
9	add this candidate point to the blacklist
10	**end if**
11	**else**
12	randomly determine a point in the μ-K plane as the candidate point
13	perform MIMO equalization for the candidate point
14	**if** BER of the candidate point < BER of the current point **then**
15	the ant moves to the candidate point
16	**else**
17	add this candidate point to the blacklist
18	**end if**
19	**end if**
20	**end for**

Algorithm 3. Random ACO-MIMO updating policy.

1	**for** $n = 1$ to N **do**
2	produce the P_{tran}^n
3	**if** $P_{tran}^n < P_0$ **then**
4	determine a point around the current point as a candidate point as presented in Figs. 2 (c) or (d)
5	perform MIMO equalization for the candidate point
6	**if** BER of the candidate point < BER of the current point **then**
7	the ant moves to the candidate point
8	**else**
9	add this candidate point to the blacklist
10	**end if**
11	**else**
12	randomly determine a point in the μ-K plane as the candidate point
13	perform MIMO equalization for the candidate point
14	**if** BER of the candidate point < BER of the current point **then**
15	the ant moves to the candidate point
16	**else**
17	add this candidate point to the blacklist
18	**end if**
19	**end if**
20	**end for**

movement direction of ants in local search is determined by the priorities illustrated in Figs. 2(a) and (b), corresponding to different arrival directions. The arrival directions are demonstrated by the black dash lines. Additionally, assuming a smooth relationship between BER and μ-K, we believe that the greater similarity between the movement direction to the next hop and the arrival direction will result in a larger reduction in BER. Therefore, in Figs. 2(a) and (b), the highest priority movement direction, indicated by the red dashed line, aligns with the arrival direction. And the angles between the movement directions of the 2nd, 3rd, and 4th priority levels and the arrival direction are 45°, 90°, and 135° respectively. This assumption facilitates the rapid location of optimal parameters for the fixed ACO-MIMO scheme under a regular BER distribution. Nonetheless, irregularities in the BER distribution can potentially lead to the fixed ACO-MIMO becoming trapped in local optima, requiring a greater number of subsequent FD-LMS iterations to break free from this predicament. To mitigate this risk, we introduce the random ACO-MIMO scheme. The movement direction priorities of random ACO-MMO in local search are depicted in Figs. 2(c) and (d). In this scheme, all directions carry equal priority, and the search step size remains 1. So that the pheromones associated with the ants performing consecutive local searches can reflect the BER levels in their vicinity. And it could ensure stable local search avoiding the entrapment of local optima. A comparative analysis of the two proposed ACO-MIMO schemes is discussed in Section 4.
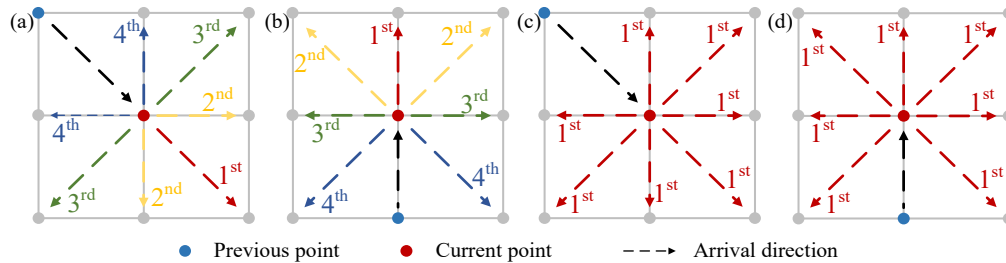

Fig. 2. Movement direction priority in local search for (a), (b) fixed ACO-MIMO, and (c), (d) random ACO-MIMO.

During evolution, ants converge towards the optimal μ-K coordinate based on the positive feedback from the updates of the pheromone concentration and the transfer probability. Among them, during the pheromone update, the evaporation coefficient introduces a form of memory into the update process of pheromone, enhancing the reliability of results in consecutive local searches. Furthermore, the ants situated at coordinates with lower BER have a greater likelihood of locating the optimal points. The update of transfer probability ensures these ants persist in their local search. Conversely, the transfer probability shifts the ants in the regions with higher BER toward the regions with higher pheromone concentrations through global search. Therefore, the joint positive feedback mechanism of transfer probability updating and pheromone updating gradually guides ants to converge towards the regions with lower BER distributions, thereby increasing the efficiency of locating the optimal coordinate.

During each evolution, ants update the μ-K coordinates based on the evolution strategy, and then call the FD-LMS algorithm to compute BER at the current coordinates. Assuming in the $D \times D$ MIMO system, during each call of the FD-LMS algorithm, it is trained $T_{\text{FD−LMS}}$ times, then the required complex multiplications $M_{\text{FD−LMS}} = T_{\text{FD−LMS}} \times [(4D + 4) \times \log_2(2K) + 8D]$ [10]. However, ACO simply compares BERs according to predefined strategies and moves the ants accordingly. The computational complexity of the ACO is significantly lower than that of FD-LMS. Hence, the critical aspect of reducing the complexity associated with locating μ-K parameters is to minimize the calling times of the FD-LMS algorithm throughout this procedure. In Section 4, we evaluate the performance of the ACO-MIMO scheme through the hit probability

of optimal parameters, the number of FD-LMS algorithm calls, and the distribution characteristics of the output BER. Additionally, for comparison purposes, we also compute the results using the GA and SDA algorithms to locate the optimal *μ-K* combination in the subsequent discussion.

3. Experimental setup of a 3-mode recirculating loop transmission system

To validate the practical performance of the ACO-MIMO scheme, we constructed a 3-mode recirculating loop transmission system. The experimental setup was consistent with our previous work [15], as illustrated in Fig. 3. The setup comprises three units: the signal generation unit, the few-mode recirculating loop unit, and the signal processing unit. In the signal generation unit, a continuous light of 1550.3 nm and a non-return-to-zero (NRZ) signal were generated by the narrow-linewidth continuous-wavelength (CW_1) laser and the arbitrary-waveform generator (AWG), respectively. Then they were injected into the IQ modulator (IQM) to generate a 10 Gbit/s optical quadrature-phase-shift keying (QPSK) signal for the 3-mode loop transmission. After undergoing optical amplification and being filtered by an erbium-doped fiber amplifiers (EDFA) and a band-pass optical filter (BPF), the optical signal was split into three branches using three 50:50 optical couplers (OCs). Each split signal was individually adjusted by its own variable optical attenuator (VOA) and polarization controller (PC) in each branch before being delivered into the few-mode recirculating loop unit.
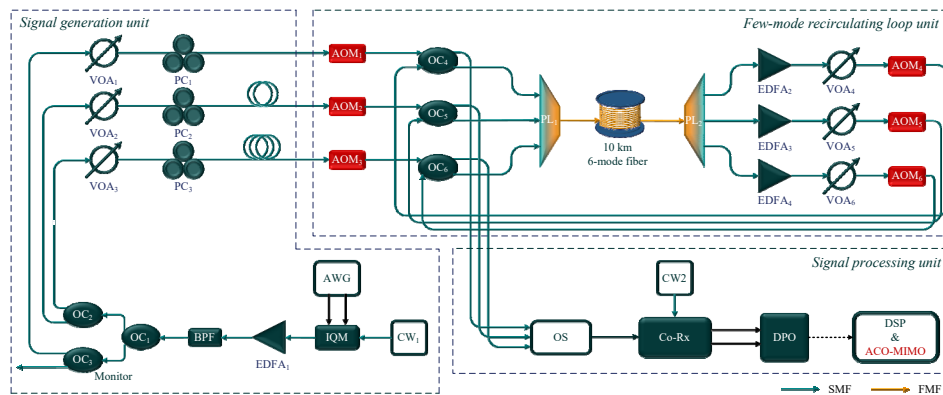

Fig. 3. Experimental setup of the 3-mode recirculating loop transmission system.

Within the few-mode recirculating loop unit, the primary functions include controlling the on-off state of the acousto-optic modulators (AOM) with precise timing, thereby determining the propagation direction for the optical signals within the loop. We set up the 3-mode recirculating loop system using multiple single-mode AOMs, with rising and falling edges in the magnitude of nanosecond, to either block or pass the signals, enabling support for 3-mode looped transmission. Additionally, 50:50 optical couplers (OC_4, OC_5, and OC_6) within the loop served as the transmission hub. One output port of each OC was linked to the few-mode converter device, while the other was responsible delivering the output signals from each round-trip to the signal processing unit. The excited few-mode optical signals through mode-selective photonic lantern (PL_1) were simultaneously coupled into a 10 km-length graded-index 6-mode fiber. It is worth noting that the mode multiplexing/demultiplexing performance of fused taper-manufactured photonic lanterns exhibits a certain dependence on polarization. And we utilized polarization controllers to ensure that the polarization state of the signals remains in the normal operating condition of the few-mode device. Then, at the output of the 6-mode fiber, the signals were demultiplexed by the PL_2 for single-mode loop operation. In MDM system, strong time-varying mode coupling can severely degrade the transmission performance of the system. Exciting only a

subset of modes to carry signal transmission could reduce the overall mode coupling strength, which is advantageous for verifying the performance of the ACO-MIMO scheme over longer transmission distances. In the testing, we found that the coupling strength between the LP_{01}, LP_{21a}, and LP_{02} modes in our system was relatively low. Therefore, we considered these three modes as the mode-division channels in our experiment, as demonstrated in [24]. The PLs and the 6-mode fiber were produced by Phoenix Photonics and YOFC [25,26], respectively. The power control via EDFAs and VOAs was implemented to maintain uniform power levels across each spatial mode. Similar to the single-mode recirculating loop system, the coordinated operation between AOM_4 to AOM_6 within the loop and AOM_1 to AOM_3 outside the loop was utilized to prevent data collisions during looped transmission.

In the signal processing unit, the output single-mode signals were selected by an optical switch (OS) one by one. And the selected signal was detected by the coherent receiver (Co-Rx) and sampled by a digital phosphor oscilloscope (DPO) with the rate of 50 GS/s. Despite this constraint, we have made significant efforts to synchronize the signals. Based on the varying delay lengths between delay lines in the signal generation unit, we calculated the symbol offset between corresponding data frames of each branch. Starting from the received frame header of each branch, we cut off the corresponding number of symbols according to the symbol offset. The new frames of each branch are then synchronized as closely as feasible. Before the MIMO equalization, the three-channel data was processed by the DSP algorithms to compensate the traditional noise, such as the IQ balance, Gardner algorithm-based time synchronization [27], Schmidl algorithm-based frame synchronization [28], and quartic method-based frequency offset estimation [29]. And then the proposed MIMO scheme integrates with a carrier phase recovery algorithm based on the Viterbi-Viterbi scheme [30] to process these data to mitigate the impact from the mode-related distortions.

4.   Results and discussions

Based on the 3-mode recirculating loop transmission system demonstrated in Section 3, we have collected data from 20 round-trips. We firstly used the collected data of the 15th round-trip to investigate the μ-K optimization performance of the proposed ACO-MIMO schemes. Before commencing the scheme, we predefined the value ranges of μ and K as $[1 \times 10^{-6}:2 \times 10^{-6}:1 \times 10^{-4}]$ and $[50:20:950]$, respectively, where 2×10^{-6} and 20 represented the step sizes. Within this range, the minimal BER could be achieved based on our experience. As each μ-K combination corresponds to a BER output, the BER distribution plane comprises 2400 coordinate points. Additionally, as a comparison algorithm, the GA algorithm, known for its effectiveness in parameter optimization, was implemented with the elite retention strategy, where the crossing probability P_c and the mutation probability P_m were set as 0.9 and 0.05, respectively [31]. During each evolution, they compared the BER of all neighboring points and moved towards the point with the minimum BER. Once all the surrounding BERs were larger than their own, the individual terminated the evolution.

Based on the description in Section 2, the transfer probability threshold P_0 serves as a critical parameter in ACO-MIMO scheme, determining the search behavior of ants. To quantify the effectiveness of the ACO-MIMO in locating the optimal parameters, we define P_{hit} as the hitting probability for the optimal μ-K coordinate, as expressed in Eq. (3). In Eq. (3), T_{test} represents the number of independent tests conducted, which was considered as 5000. And T_{hit} represents the number of times the optimal coordinate was hit. Figures 4(a) and (b) respectively depict the relationships between P_{hit} and the evolution times G under different P_0 values in fixed and random ACO-MIMO. The number of ants in Figs. 4(a) and (b) was fixed as 20. For both ACO schemes, when P_0 is $5e^{-4}$, they exhibit the highest convergence speed and converged value of P_{hit} as G increases. Therefore, in subsequent discussions, P_0 is set to $5e^{-4}$.
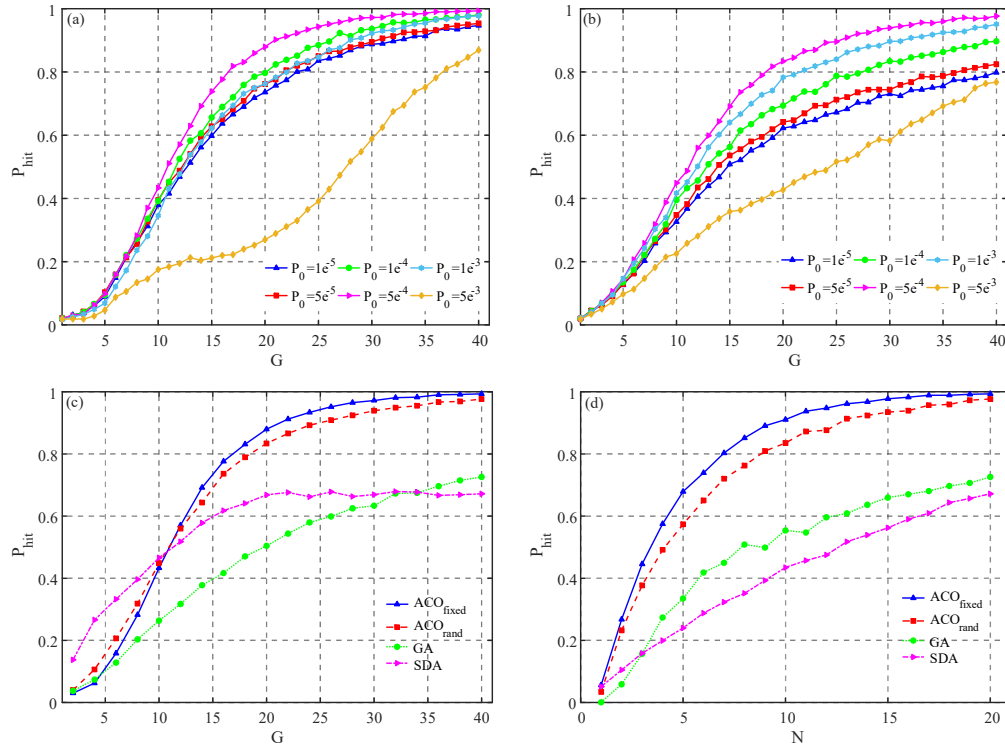
Fig. 4. Evolution of P_{hit} with G under varying P_0 for (a) fixed and (b) random ACO-MIMO; evolution of P_{hit} with (c) G and (d) N for each algorithm. (In ACO-MIMO, GA, and SDA, N represents the number of ants, individuals, and parallelly optimized coordinates, respectively.)

Figures 4(c) and (d) depict the variations of the P_{hit} as a function of G and N for different schemes, respectively. In Fig. 4(c), N for the four algorithms was fixed at 20. Initially, with small values of G, the P_{hit} for each algorithm remained low. During the early stages, SDA exhibited a relatively higher P_{hit} due to its rapid local search capability [32]. However, as G exceeded 10, the benefits of local search in SDA became saturated, and the P_{hit} surpassed by the proposed ACO algorithms. Additionally, the superior search capability of the ACO algorithms led to a significant gap in P_{hit} compared to the GA and SDA algorithms. Specifically, when G = 40, the P_{hit} values for the fixed ACO, random ACO, GA, and SDA algorithms were 99.34%, 97.7%, 72.6%, and 67.18%, respectively. For Fig. 4(d), the evolution times G was fixed at 40. Similarly, with small N, the search performance of the algorithm was not fully utilized, resulting in lower P_{hit} values. As N gradually increased, the proposed ACO algorithms widened the gap in P_{hit} compared to the comparison algorithms and tended to converge after N > 15.

$$P_{hit} = \frac{T_{hit}}{T_{test}}. \tag{3}$$

Based on the analysis above, it's evident that the optimal μ-K combination may not be achieved with these schemes. To quantify the complexity of the proposed schemes, we introduce C_{LMS}, which represents the number of times the FD-LMS algorithm needs to be called to achieve the optimal μ-K combination once. This metric can be computed using Eq. (4), where C_{mean} denotes the average number of calls to the FD-LMS algorithm across T_{test} tests. In Table 1, we demonstrate the theoretical C_{mean} of each algorithm under fixed G, N and the measured C_{mean}

over 5000 tests at G = 40 and N = 20. The low C_{mean} of 820 is achieved by the proposed fixed and random ACO-MIMO, which is only about 40% compared to SDA. In the SDA algorithm, to obtain the lowest BER around each individual, it requires a significant number of calls to the FD-LMS algorithm in every evolution. It should be also noticed that although the GA approach achieves the lowest C_{mean}, its lower P_{hit} leads to a higher BER output, see the green lines in Figs. 4(c) and (d). Therefore, compared to the conventional SDA and GA algorithms, the proposed fixed and random ACO-MIMO could achieve the best signal output with the less computation complexity.

$$C_{\text{LMS}} = \frac{C_{\text{mean}}}{P_{\text{hit}}} = C_{\text{mean}} \times \frac{T_{\text{test}}}{T_{\text{hit}}}. \tag{4}$$

Table 1. Theoretical and Measured C_{mean} for different algorithms with G = 40 and N = 20.

	Fixed ACO-MIMO	Random ACO-MIMO	GA	SDA
Theoretical C_{mean}	$N + N \times G$	$N + N \times G$	$N + (N-1) \times G$	$< 8 \times N \times G$
Measured C_{mean}	820	820	780	2040

To illustrate the computational complexity performance of the proposed schemes, the required C_{LMS} for each algorithm as G and N increase is depicted in Figs. 5(a) and (b), respectively. In both figures, it is observed that the required C_{LMS} initially decreases and then increases. This trend can be explained by the fact that during the initial stages, the increasing speed of T_{hit} is faster than that of C_{mean} (the average number of calls to the FD-LMS algorithm) due to insufficient search. Subsequently, as P_{hit} converged, further increases in G or N elevated the C_{mean} of the scheme and consequently increased the required C_{LMS}. The black dashed lines in Figs. 5(a) and (b) represent the results of the traverse search algorithm (TSA). Since there are 2400 coordinate points on the μ-K plane, after traversing all coordinate points (i.e., $C_{\text{mean}} = 2400$), the TSA algorithm could definitely hit the optimal parameter combination (i.e., $P_{\text{hit}} = 1$). Therefore, the required C_{LMS} for the TSA algorithm remains fixed at 2400. Due to the SDA algorithm's limited global search capability, when its P_{hit} converges to a lower value, the evolutionary behavior mentioned in Section 2 significantly increases the required C_{LMS}, even surpassing that of the TSA. In Fig. 5(a), the fixed ACO-MIMO scheme reduced the required C_{LMS} by 42.74%, 80.63%, and 81.93% compared to the minimum C_{LMS} for the GA, SDA, and TSA algorithms, respectively. Similarly, the random ACO-MIMO algorithm reduced the required C_{LMS} by 39.03%, 79.37%, and 80.76%, respectively. In Fig. 5(b), the fixed ACO-MIMO scheme reduced the required C_{LMS} by 39.12%, 85.66%, and 88.5% compared to the minimum C_{LMS} for the GA, SDA, and TSA algorithms, respectively. Likewise, the random ACO-MIMO scheme reduced the required C_{LMS} by 27.98%, 83.04%, and 86.4%, respectively.

The third aspect of performance measurement pertains to the distribution characteristics of the BER output. In the 5000 independent tests conducted, the mean BER outputs of each algorithm were plotted against the increasing values of G and N in Figs. 6(a) and (b), respectively. The results depicted in these figures were obtained with a fixed N of 20 and a fixed G of 40, respectively. From Fig. 6(a), it is evident that after full evolution (sufficient N and G), the high P_{hit} achieved by the ACO-MIMO schemes contributed to reducing the mean BER results, bringing them closer to the minimum BER (BER_{min}). Additionally, Fig. 6(b) exhibits a similar trend, with ACO-MIMO showing smaller BER outputs during the initial stages of evolution. This suggests that under the same evolutionary cost, i.e., with the same G and N, the ACO-MIMO schemes achieve higher population quality compared to GA or SDA. Moreover, in order to quantify the distribution of the output BER, we depicted the normal distributed probability density function (PDF) in Fig. 7 for the BER of each algorithm in 5000 tests. The PDFs of the fixed ACO and random ACO exhibited smaller standard deviations of 8.35×10^{-6} and 1.7×10^{-5}, respectively, compared to those of the GA and SDA algorithms, which were 5.25×10^{-5} and 1.04×10^{-4},
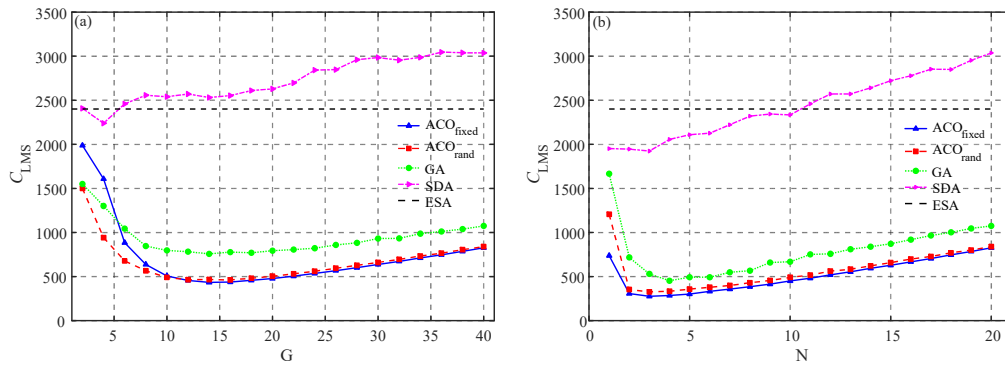
Fig. 5. Evolution of required C_{LMS} with (a) G and (b) N for each algorithm. (In ACO-MIMO, GA, and SDA, N represents the number of ants, individuals, and parallelly optimized coordinates, respectively.)

respectively. Additionally, the mean values of the ACO-MIMO PDFs were closer to BER_{min}. This is significant for long-term communication to maintain system stability.

To evaluate the performance of the ACO-MIMO schemes across various transmission distances, we implemented them using data collected from different round-trips. The results are illustrated
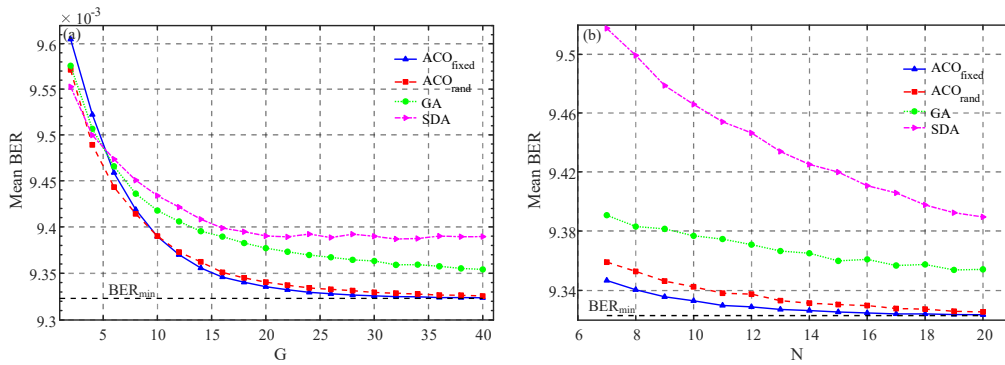

Fig. 6. Evolution of mean BER with (a) G and (b) N for each algorithm. (In ACO-MIMO, GA, and SDA, N represents the number of ants, individuals, and parallelly optimized coordinates, respectively.)
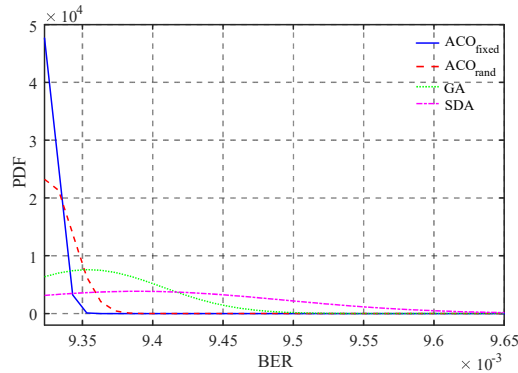

Fig. 7. PDF of BER outputs for each algorithm with G = 40 and N = 20.

in Fig. 8, where G = 40 and N = 20. Each marker represents the average outcome of 25 data sets. Figure 8(a) demonstrates the P_{hit} for each round-trip. For the first round-trip, the P_{hit} of each algorithm was high. This is attributed to the high signal quality of the collected data, where multiple μ-K combinations resulted in the same BER output of 0, facilitating the hitting of optimal parameters. The increase in transmission distance enlarged the performance gap between the various algorithms. During the recirculating-loop transmission, the P_{hit} of ACO-MIMO consistently outperforms that of GA and SDA algorithms. The required C_{LMS} for each algorithm across different round-trips is depicted in Fig. 8(b). The C_{LMS} results for SDA were not included due to their excessively high values (over 4000), making them impractical to plot in a single figure. It can be observed that, except for small round-trips, the C_{LMS} required for ACO-MIMO schemes is generally lower than that required for the GA algorithm in most cases. On the 6th round-trip, the fixed and random ACO-MIMO schemes respectively reduced the required C_{LMS} by up to 28.97% and 26.16% compared to the GA algorithm. Additionally, due to the time-varying nature of channel states in MDM systems, signals collected under different round-trips and datasets were affected by varying degrees of mode-related distortions. This is what causes the results of each algorithm in Fig. 8 to fluctuate up and down with the round-trip. However, after statistical analysis of multiple independent tests, the evident difference between the P_{hit} and C_{LMS} of each algorithm is able to characterize the performance gap between them.
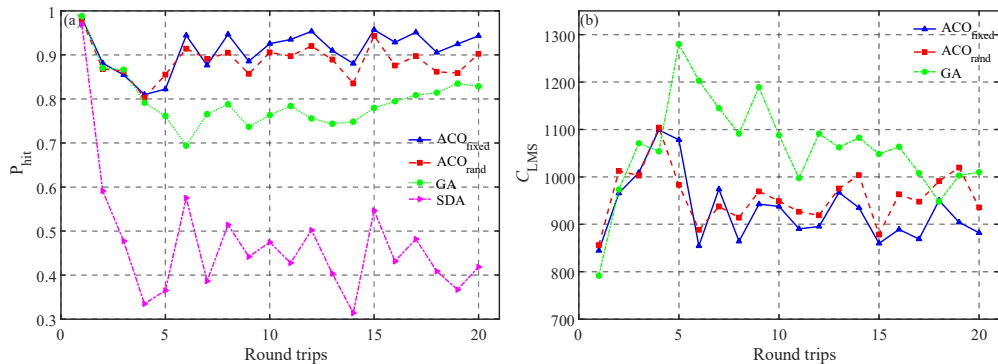

Fig. 8. (a) P_{hit} and (b) C_{LMS} for each algorithm from the 1st to 20th round-trip.

As described in Section 2, the difference between the fixed ACO-MIMO and the random ACO-MIMO comes from the principle of local search. Therefore, the performance gap between the two schemes heavily depends on the operation scenarios. In Fig. 9, we compare the performance of the two algorithms under different BER distribution scenarios. The data in the figure is sourced from the experimental results of the 20th round-trips. Specifically, Fig. 9(a) demonstrates superior performance for fixed ACO-MIMO, whereas in Fig. 9(b), random ACO-MIMO exhibits better performance. Additionally, in Figs. 9(a) and (b), we present the respective local BER distribution plots, with red triangle markers indicating the coordinate points corresponding to the minimum BER. According to the BER distribution shapes in the two figures, we define the distribution in Fig. 9(a) as the flat distribution, where there is no local optimum near the optimal point, and the distribution in Fig. 9(b) as the undulating distribution with the clear local optima. Combining the performance curves in Fig. 9 with the local search strategies of the two algorithms, we observe that the flat distributed BER plane is advantageous for the ants in the fixed ACO-MIMO scheme to converge quickly to the optimal parameter point. In the case of an undulating distributed BER plane, the fixed ACO-MIMO scheme requires a greater evolutionary cost to escape local optima traps. Consequently, the undulating distribution is better suited for the random ACO-MIMO scheme, which exhibits faster escape from local optima. Although both ACO-MIMO schemes

have distinct advantages, as indicated by the analysis of Fig. 8, there is no notable performance gap between them across multiple sets of data during the 20 round-trip transmissions. This suggests that when deployed with substantial practical data featuring diverse BER distributions, the overall performance of the two proposed ACO-MIMO schemes is nearly identical.
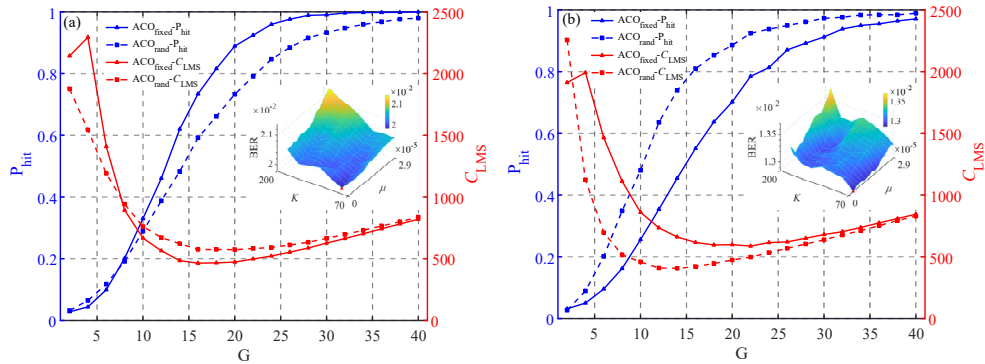

Fig. 9. Performance comparison of two ACO-MIMO schemes under (a) flat and (b) undulating BER distribution.

5. Conclusion

We proposed the fixed ACO-MIMO and random ACO-MIMO schemes to efficiently locate optimal MIMO equalization parameters. We validated the performance of these schemes using a 3-mode recirculating transmission loop system. Our results demonstrate that compared to GA and SDA algorithms, the proposed ACO-MIMO schemes significantly reduced the C_{LMS} by up to 42.74% and 80.63%, respectively, achieving a maximum P_{hit} of 99.34% and generating more concentrated BER outputs. Additionally, when tested with data from 20 round-trips, both fixed ACO-MIMO and random ACO-MIMO schemes reduced the C_{LMS} required by the GA algorithm by up to 28.97% and 26.16%, respectively. Finally, our analysis of performance under various BER distributions reveals that while each scheme has its strengths, their overall performance is nearly equivalent when applied to extensive test data.

Disclosures. The authors declare no conflicts of interest.

Data availability. Data underlying the results presented in this paper are not publicly available at this time but may be obtained from the authors upon reasonable request.

References

1. D. Richardson, J. Fini, and L. Nelson, "Space-division multiplexing in optical fibres," Nat. Photonics **7**(5), 354–362 (2013).
2. G. Li, N. Bai, N. Zhao, *et al.*, "Space-division multiplexing: the next frontier in optical communication," Adv. Opt. Photon. **6**(4), 413–487 (2014).
3. P. J. Winzer, "Optical Networking Beyond WDM," IEEE Photonics J. **4**(2), 647–651 (2012).
4. K. Shibahara, T. Mizuno, D. Lee, *et al.*, "Advanced MIMO signal processing techniques enabling long-haul dense SDM transmissions," J. Lightwave Technol. **36**(2), 336–348 (2018).
5. T. Sakamoto, T. Mori, T. Yamamoto, *et al.*, "Mode-division multiplexing transmission system with DMD-independent low complexity MIMO processing," J. Lightwave Technol. **31**(13), 2192–2199 (2013).
6. F. Tian, T. Wu, C. Yu, *et al.*, "Kramers–Kronig transmission with a crosstalk-dependent step multiple-input multiple-output Volterra equalizer in a seven-core fiber," Photonics **10**(9), 1017 (2023).

7. X. Chen, J. He, A. Li, *et al.*, "Characterization and Analysis of Few-Mode Fiber Channel Dynamics," IEEE Photonics Technol. Lett. **25**(18), 1819–1822 (2013).

8. K. Choutagunta and J. M. Kahn, "Dynamic Channel Modeling for Mode-Division Multiplexing," J. Lightwave Technol. **35**(12), 2451–2463 (2017).

9. W. Yu, Z. Yang, X. Wang, *et al.*, "Frequency-domain VFF-RLS equalization for the time-varying mode-division multiplexed channels," *CLEO*, 2020, paper JTu2E.7.

10. G. Hu and C. Huang, "A variable step-size unconstrained adaptive FD-LMS algorithm for MDM transmission," IEEE Photonics J. **10**(2), 7201512 (2018).

11. F. Pittalà, A. Zanaty, F. J. V. Caballero, *et al.*, "Training-aided 6×6 MIMO frequency-domain equalizer for optical SDM transmission systems," *IEEE Photonics Conference*, 2016, pp. 523–524.

12. X. He, Y. Weng, and Z. Pan, "A step-size controlled method for fast convergent adaptive FD-LMS algorithm in few-mode fiber communication systems," J. Lightwave Technol. **32**(10), 3820–3826 (2014).

13. R. G. H. van Uden, C. M. Okonkwo, V. A. J. M. Sleiffer, *et al.*, "MIMO equalization with adaptive step size for few-mode fiber transmission systems," Opt. Express **22**(1), 119–126 (2014).

14. D. Xu, B. Yin, W. Wang, *et al.*, "Variable tap-length LMS algorithm based on adaptive parameters for TDL structure adaption," IEEE Signal Processing Lett. **21**(7), 809–813 (2014).

15. T. Zhao, F. Wen, S. Tang, *et al.*, "All-fiber mode-division-multiplexed recirculating-loop transmission system with ultralow-cost MIMO algorithm," *OECC*, 2023.

16. V.A.J.M. Sleiffer, Y. Jung, V. Veljanovski, *et al.*, "73.7 Tb/s (96 × 3 × 256-Gb/s) mode-division-multiplexed DP-16QAM transmission with inline MM-EDFA," Opt. Express **20**(26), B428–B438 (2012).

17. F. Pittalà, F. N. Hauske, Y. Ye, *et al.*, "Data-aided frequency-domain 2 × 2 MIMO equalizer for 112 Gbit/s PDM-QPSK coherent transmission Systems," *OFC*, 2012, paper OM2 H.4.

18. F. M. Ferreira and F. A. Barbosa, "Towards 1000-mode optical fibres," arXiv, (2022).

19. J. Tang, G. Liu, and Q. Pan, "A review on representative swarm intelligence algorithms for solving optimization problems: applications and trends," IEEE/CAA J. Autom. Sinica **8**(10), 1627–1643 (2021).

20. X. Guo, H. Y. Zhou, S. Guo, *et al.*, "Design of broadband omnidirectional antireflection coatings using ant colony algorithm," Opt. Express **22**(S4), A1137–A1144 (2014).

21. M. D. Toksari, "Ant colony optimization for finding the global minimum," Applied Mathematics and Computation **176**(1), 308–316 (2006).

22. S. U. Seçkiner, Y. Eroğlu, M. Emrullah, *et al.*, "Ant colony optimization for continuous functions by using novel pheromone updating," Applied Mathematics and Computation **219**(9), 4163–4175 (2013).

23. L. Yang, X. Ke, R. Bai, *et al.*, "Adaptive tracking and compensation of laser spot based on ant colony optimization," Proc. SPIE **7283**, 728329 (2009).

24. M. Zuo, D. Ge, Y. Gao, *et al.*, "3-mode real-time MDM transmission using single-mode OTN transceivers over 300 km weakly-coupled FMF," *OFC*, 2022, paper M4B.4.

25. http://www.phoenixphotonics.com/website/products/documents/Photonic%20Lantern%20V2.0_01706.pdf.

26. https://en.yofc.com/view/2351.html.

27. F. Gardner, "A BPSK/QPSK Timing-Error Detector for Sampled Receivers," IEEE Trans. Commun. **34**(5), 423–429 (1986).

28. T. M. Schmidl and D. C. Cox, "Robust frequency and timing synchronization for OFDM," IEEE Trans. Commun. **45**(12), 1613–1621 (1997).

29. A. Leven, N. Kaneda, U. -V. Koc, *et al.*, "Frequency Estimation in Intradyne Reception," IEEE Photonics Technol. Lett. **19**(6), 366–368 (2007).

30. A. J. Viterbi and A. M. Viterbi, "Nonlinear estimation of PSK-modulated carrier phase with application to burst digital transmission," IEEE Trans. Inf. Theory **29**(4), 543–551 (1983).

31. W. Wang, G. Ning, L. Pei, *et al.*, "Gain equalization of few-mode fiber amplifier based on genetic algorithm," Chinese Journal of Lasers **41**(9), 27–34 (2021).

32. A. M. Burden, R. L. Burden, and J. D. Faires, *Numerical Analysis*, 10th ed.; (Cengage, 2016), Chap. 10.